World Journal of Advanced Engineering Technology and Sciences
eISSN: 2582-8266
Cross Ref DOI: 10.30574/wjaets
Journal homepage: https://wjaets.com/

(RESEARCH ARTICLE)

Pyrolysis of raffia palm fronds in a fixed bed reactor: process optimization and bio-oil characterization

Vivian Chinenye Akunne *, A.E. Ochonogor and Paul Madus Ejikeme

Department of Pure and Industrial Chemistry, Physical sciences, University of Nigeria Nsukka, ENUGU State, Nigeria.

World Journal of Advanced Engineering Technology and Sciences, 2025, 16(02), 390-402

Publication history: Received on 13 July 2025; revised on 23 August 2025; accepted on 25 August 2025

Article DOI: https://doi.org/10.30574/wjaets.2025.16.2.1294

Abstract

A fixed bed reactor was designed, fabricated and used for raffia frond pyrolysis. This work focused on the study of the effect of temperature and time on pyrolysis of raffia fronds using response surface methodology (RSM). The ultimate and proximate analysis as well as thermogravimetric analysis (TGA) were performed to determine the chemical and thermal properties of the biomass fronds. The optimum pyrolysis oil conditions were temperature of 700 ^{o}C, and time of 75 min with a corresponding liquid yield of 52.31 wt %. Model validation using coefficient of determination (R^2) was 0.6985. The extracted Pyrolysis oil was also characterized by physiochemical analysis, ultimate analysis and chemical components using FTIR and GC-MS found in bio-oil were also identified. In FTIR examination of all the functional groups found that oxygen predominates in the chemical component. While for the GC-MS, it was noted that the bio-oil's chemical composition corresponds to a mixture of several aromatic and oxygenated molecules, such as aldehydes, phenols, ketones, and carboxylic acids.

Keywords: Pyrolysis; Bio-oil; Response surface methodology (RSM); Raffia palm frond; Biomass

1. Introduction

The primary source of energy in the world is fossil fuels, and the non-stop use of these fossil fuels is diminishing them as well as also contributing to global warming (Bhatia *et al.,* 2021). The price of fossil fuels is rising in cycle with the rise in energy demand. By 2030, Asia's energy demand, the most populous landmass- will rise by 76%, according to a report by the International Energy Agency (Bhatia *et al.,* 2021). All nations' energy security and economic stability are thus seriously threatened by their reliance on imported fossil fuels, since the world is predicted to run out of petroleum within the next 50 years (Bhatia *et al.,* 2021). There is a lot of study being done on the quest for alternative energy sources because of the finite supply of traditional fossil fuels and their negative effects on the climate and human health. Biomass is a cutting-edge renewable energy source with nearly zero net carbon dioxide (CO_2) emissions into the atmosphere. Amongst the push for clean energy and fossil fuels, the active use of biomass as a source of clean energy has gathered a lot of study interest recently. The International Energy Agency (IEA) estimated that in 2009 biomass was almost 10% of the world's total primary energy supply (IEA, 2023). Raffia and raffia fronds, which are primarily from tropical Africa and Madagascar can be utilized as a substitute energy source because they are normally produced as waste by the process of cutting and growing plants (CBBR, 2010). Growing up to 16 meters and 3 meters broad, the raffia palm fronds (Raphia) are a genus of roughly 20 palm species that are native to tropical regions of Africa and mostly Madagascar.

Due to its varied origins and species, biomass has a wide range of physical and chemical properties. From a chemical view, it is made up of several long-chain hydrocarbons containing functional groups like hydroxyl and carboxyl, while structurally it is composed of lignin, cellulose, hemicellulose, extractives, and inorganics. Biochemical and

* Corresponding author: Vivian Chinenye Akunne

thermochemical are two processes of converting biomass into fuel. Anaerobic fermentation or digestion employing bacteria is the biochemical process involved (Bridgwater, 2012). Thermochemical reactions occur in thermal environments and result in the production of solid, liquid, and gaseous products. According to (Cardoso *et al.,* 2016), Pyrolysis, gasification, combustion techniques and liquefaction are frequently used in thermal conversions while pyrolysis is widely used among all.

Pyrolysis process is the thermal breakdown of substances that contain little or no oxygen. Depending on the conditions, it converts biomass into char, gases, and bio-oil (Wang *et al*., 2023). In this pyrolysis process, several crops have been used as renewable sources for the conversion of biomass into high-value energy resources for liquid fuels production. The high oxygen content and thermal instability present in the bio-oils must be carried out by additional processing, such as catalytic pyrolysis (Pinheiro *et al.,* 2019).

2. Materials and methods

2.1. Methods

Biomass pyrolysis was performed in an electrically heated fixed bed reactor using 1 mm feedstock. The system was purged with nitrogen to create an inert atmosphere, then heated at 100 °C/min for at least 25minutes. Condensable gases were collected in ice-cooled traps, and non-condensable gases passed through a water bath. After cooling, the setup was weighed before and after to calculate yields of char, bio-oil, and gas. The dark-colored bio-oil was transferred to sample bottles, and residual oil was rinsed with ethanol.

Proximate analysis was performed on the raw material to determine moisture content, volatile matter content, ash percentage and the percentage of fixed carbon and this Analysis was conducted according to the standards provided by the American Society for Testing and Materials (ASTM). The characterization of the elements (ultimate analysis) was done to determine the percentage of carbon, hydrogen, nitrogen, sulphur and oxygen in the raw material. During this analysis, the percentage of carbon, nitrogen, and sulphur were done while that of hydrogen and oxygen was obtained by calculation (Sengar *et al.,* 2012).

The proximate and ultimate analysis results of palm fronds are shown on Table1

Thermal gravimetric analysis/Differential Thermal Analysis (TGA/DTA) also was conducted to get information for the thermal decomposition of raffia frond; thus, the temperature operation of pyrolysis process could be decided. The thermal stability data were collected on a PerkinElmer TGA 4000 made in Netherlands. The temperature was swept from 30 ^{o}C to 950 ^{o}C for sample of 7.793 mg for raffia frond. The samples were placed in an aluminum pan at a heating rate of 10.00 ^{o}C/min under nitrogen atmosphere.

Fourier Transform Infrared Spectroscopy (FTIR) also was conducted on the bio-oil to get functional groups and chemical bonds, The FTIR spectra were recorded in the range of 4000–400 cm^{-1} using a Nicolet iS10 and a Pelkin Elmer 3000 MX spectrometer. Samples were prepared by mixing a small amount of the material with KBr, grinding it into a fine powder in an agate mortar, and pressing it into pellets under 7 tons of pressure for analysis.

The bio-oil samples from the raffia frond were characterized by Gas Chromatography - Mass Spectrometry using a Perkin Elmer Turbo Mass Spectrophotometer (Norwalk, CT06859, and USA) which includes a Perkin Elmer Auto sampler XLGC. The column used was the Perkin Elmer Elite-5 capillary column measuring 30 m x0.25 mm with a film thickness of 0.25 mm composed of 95 % Dimethyl polysiloxane. The carrier gas used was helium at a flow rate of 0.5ml/min. 1µl sample injection volume was utilized.

The optimization of bio-oil production using response surface modeling (RSM) was carried out using Design Expert (version 11.0). A full-factorial Central Composite Design (CCD), involving two independent variables at three levels, was employed. In these experiments for the response of bio-oil yield, the two factors considered were reaction temperature and reaction time having three stage factors: -1, 0 and +1, α value depending on the number of factors in the factorial design as shown in equation 2.1.

$$\alpha = [2^n]^{1/4} \qquad (2.1)$$

Where

n = number of factors studied; α = 1.68.

Reaction temperature and reaction time were coded as A, B respectively. The two factors were bound between the lower and upper limiting values. The lower coded limit for each factor was −1 while the upper coded limit for each factor was +1. A complete description of each factor, its low and high actual value with coded lower and upper value is given in Table 1

Table 1 Ranges of independent process variables and experimental levels with their actual and coded values for the pyrolysis of Raffia palm frond (RPF)

Process variables	**Symbol**	**Coded levels**		
		-1	0	+1
Temperature (°C)	A	600	650	700
Time (min)	B	50	62.5	75

Table 2 Characteristics of the Raffia Frond (RF)

Proximate analysis (wt. % dry basis)	
Ash	2.4
Fixed carbon	0.16
Moisture content	7.4
Volatile matter	90.04
Ultimate analysis (wt. % dry basis)	
Carbon	45.61
Hydrogen	7.57
Nitrogen	0.206
Sulphur	0.68
Oxygen	45.94
Calorific value (MJ kg-1)	30.16

3. Results and discussion

3.1. Thermogravimetric analysis of Raffia frond (RF)

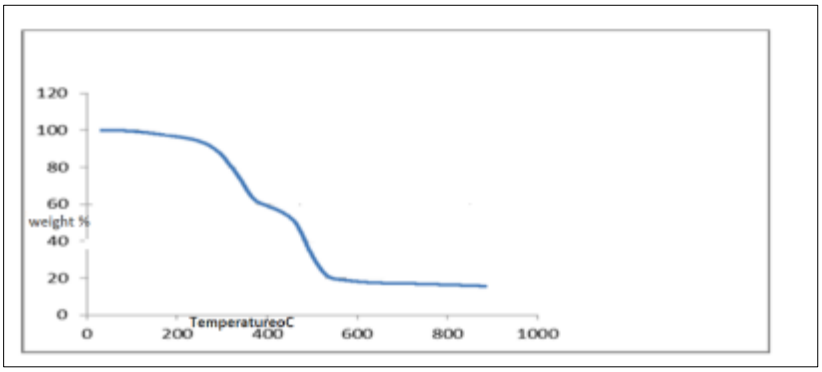

Figure 1 TGA curve for RF pyrolyzed at a heating rate of 10.00 °C/min

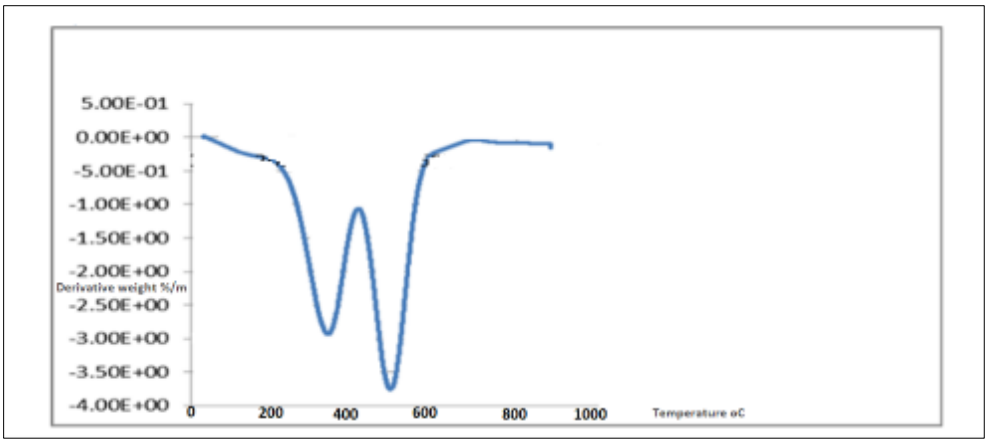

Figure 2 DTG curve for RF pyrolyzed at a heating rate of 10.00 °C/min

The TGA curve in Figure 1 shows a gradual weight loss of 100 C to 250 °C occurring due to moisture evaporation and hemicellulose decomposition. A significant mass loss of 66.94 wt% occurs between 300.20 °C and 550.11 °C due to primary devolatilization and the release of carbon and volatiles. Between 550.11 °C and 900 °C, the weight loss continues more gradually, with 15.621 wt% char remaining at the end of pyrolysis.

In figure 2 the DTA curve shows two thermal peaks at 360 °C and 500 °C, which indicates that decomposition was taking place. While at 600 °C, there was a further loss of mass, and it occurs due to changes in the char structure and also breakdown of the lignin which is possibly accompanied with ash transformation (Fan *et al.,* 2017).

3.2. Experimental Design with RSM

3.2.1. Screening experiment on pyrolysis of RPF

Table 3 Results of screening experiment on pyrolysis oil

Standard order of runs	Randomised order of Runs	Reaction temperature (°C)	Reaction time (min)	Bio-oil yield (wt%) Actual	Bio-oil yield (wt%) Predicted
1	11	0 (650)	0 (62.5)	46.30	47.66
2	12	0 (650)	0 (62.5)	47.35	47.66
3	8	0 (650)	1 (75)	49.43	49.95
4	7	0 (650)	-1 (50)	44.15	45.37
5	3	-1 (600)	1 (75)	47.45	47.59
6	5	-1 (600)	0 (62.5)	47.70	45.29
7	9	0 (650)	0 (62.5)	44.98	47.66
8	13	0 (650)	0 (62.5)	47.80	47.66
9	4	1 (700)	1 (75)	52.70	52.31
10	6	1 (700)	0 (62.5)	49.55	50.02
11	10	0 (650)	0 (62.5)	50.45	47.66
12	1	-1 (600)	-1 (50)	42.30	45.00
13	2	1 (700)	-1 (50)	49.38	47.72

The result showed that the predicted and actual bio-oil yields were very close to each other, suggesting a strong relation between the predicted model and its actual result and thus model can be used to predict the pyrolysis oil yield. The highest actual yield obtained was 52.70 wt% while predicted yield gave the highest amount to be 52.31 wt% at reaction temperature of 700 °C and reaction time of 75 min. The actual values of the two independent variables (A and B) and

the response (bio-oil yield) were used to develop a model equation. Equation 3.1 in terms of coded factors and Equation 3.2 in terms of actual factors for the bio-oil yield (wt%) was used to fit experimental data to the linear model.

$$Bio\ Oil\ yield\ (wt\%) = +47.66 + 2.36A + 2.29B \qquad (3.1)$$

$$Bio\ Oil\ yield\ (wt\%) = +5.4726 + 0.047267\ Reaction\ temperature\ (^0\text{C}) + 0.183333\ Reaction\ time\ (\text{min}) \quad (3.2)$$

3.2.2. Regression analysis and ANOVA of Pyrolysis of RPF for Bio-Oil Production

Table 4 Analysis of Variance of Pyrolysis of RPF for Bio-Oil Production

Source	Sum of Squares	Df	Mean Square	F- value	p-value	
Model	65.02	2	32.51	11.58	0.0025	significant
A-temp	33.51	1	33.51	11.94	0.0062	
B-time	31.51	1	31.51	11.23	0.0074	
Residual	28.07	10	2.81			
Lack of Fit	11.54	6	1.92	0.4655	0.8077	not significant
Pure Error	16.53	4	4.13			
Cor Total	93.09	12				

The interaction between the independent variables as well as significance of each model term were established using the analysis of variance (ANOVA). Any linear model must pass the Fischer test value (F-value) and probability value (p-value) in order to be accepted. While a lower p-value denotes a model's higher relevance, a higher F-value value shows the model's stronger reliability (Sarve *et al.,* 2015). The Model F-value of 11.58 indicates that the model is statistically significant. This means that there is only a 0.25% probability that such a large F-value could be due to random noise, suggesting the model's terms have a real effect on the response. From Table 4 it was observed that the significant model terms were both A and B with corresponding F-values of 11.94 and 11.23. This indicates that reaction temperature and reaction time significantly affect the yield as they have very small P-values less than 0.0500. The F-value is employed to find out whether two populations' means differ considerably from one another. The P-value is the probability of getting the observed results of a test assuming that the null hypothesis is correct. It is used as an alternative to reject points and to provide the smallest level of significance at which the null hypothesis would be rejected. The P-value is determined by the F-statistics and is the probability that results could have happened by chance. Given the pure error, the F-value for lack of fit, which is 0.47, suggests that the lack of fit is not substantial. A significant Lack of Fit F-value has an 80.77% probability of being caused by noise

3.2.3. Model summary fit statistics

In the Model summary statistics, it shows that standard deviation is 1.68, the mean is 47.66, the coefficient of variation (C.V.) is 3.52%, the R-squared value is 0.6985, the adjusted R-squared is 0.6382, the predicted R-squared is 0.5363, and the adequate precision is 11.5676.

The standard deviation for the bio-oil yield was 1.68. An acceptable standard deviation (SD) is one that is very minute, as this indicates that the model fits greatly to the optimization. The yield's mean response was 47.66. The relative SD of the experiment is measured by the co-efficient of variation which also displays the error as a mean percentage. Coefficient of variation is calculated by dividing the standard deviation of the anticipated response by the mean value of the observed response. Regression model with low C. V. % (less than 10 %) are more reliable and have strong repeatability. The co-efficient of determination (R^2) is 0.6985 which indicates that the model fits the data well. Other additional parameters taken into account in an ANOVA analysis including adjusted R^2 and predicted R^2. While adjusted R^2 increases the Predicted R^2 by adjusting the model parameters, thereby accounting for the number of predictors in the model. Predicted R^2 shows the divergence among the new data points explained by the regression model. The modified R^2 for the liquid yield was 0.6382, while the projected R^2 was 0.5363. The corrected R^2 of 0.6382 and the predicted R^2 of 0.5363 differ by less than 0.2, suggesting that both agree reasonably. Adequate precision measures the signal to noise ratio. A ratio greater than 4 is desirable. The ratio of 11.5676 indicates an adequate signal. This model can be used to navigate the design space. The nearer the R^2 value is to one, the better the findings, as it indicates the

degree to which the model matches the data. This suggests that this model is capable of explaining, analyzing or evaluating 69.85 % of the data.

Table 5 presents the coefficients in terms of coded factors.

Table 5 Coefficients in terms of coded factors

Factor	Coefficient Estimate	Df	Standard Error	95% CI Low	95% CI High	VIF
Intercept	47.66	1	0.4647	46.62	48.69	
A-temp	2.36	1	0.6840	0.8393	3.89	1.0000
B-time	2.29	1	0.6840	0.7677	3.82	1.0000

The coefficients estimate give the expected change in response per unit change in factor value when every other factor is held constant. The total average response of all the runs is the intercept in an orthogonal design. Based on the factor choices, the coefficients represent modifications made around that average. Variance inflation factors (VIFs) are one when the factors are orthogonal; VIFs larger than one signifies multi-co linearity; the higher the VIF, the more severe the factor correlation. VIFs of fewer than 10 are generally acceptable. Figure 3 displays the residuals map for the diagnostic analysis that is entirely by normal probability.

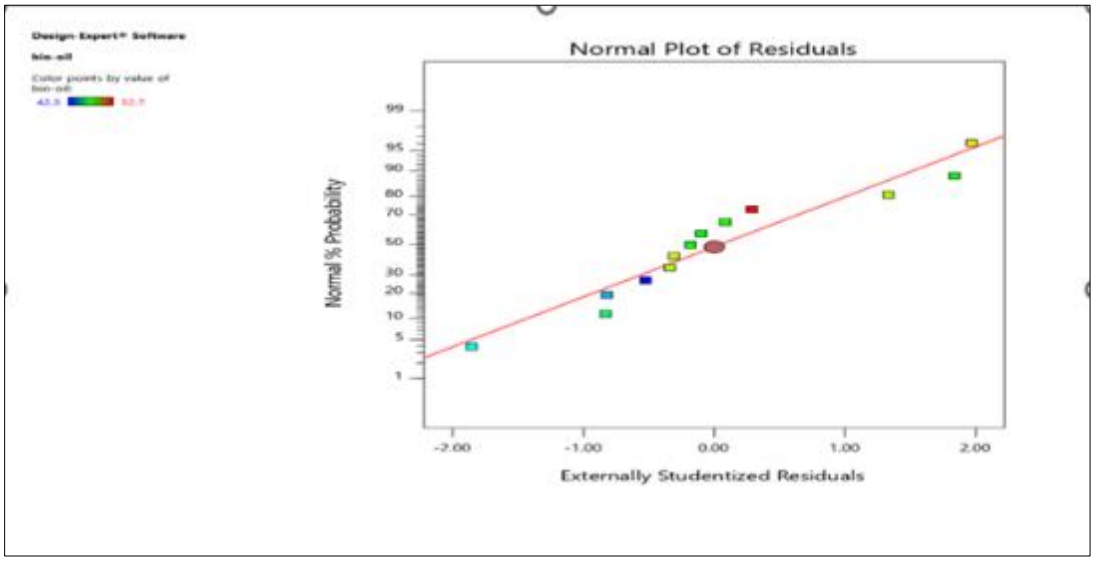

Figure 3 Normal Plots of Residuals

Considering only a small number of locations that are very slightly dispersed outside the diagonal line, it is clear from the plot that a normal distribution pattern exists, with the points of the normal distribution generally interlocked with straight lines. Figures 3 and 4, respectively, display the variance of the residuals in comparison to the expected values and the particular experimental runs.

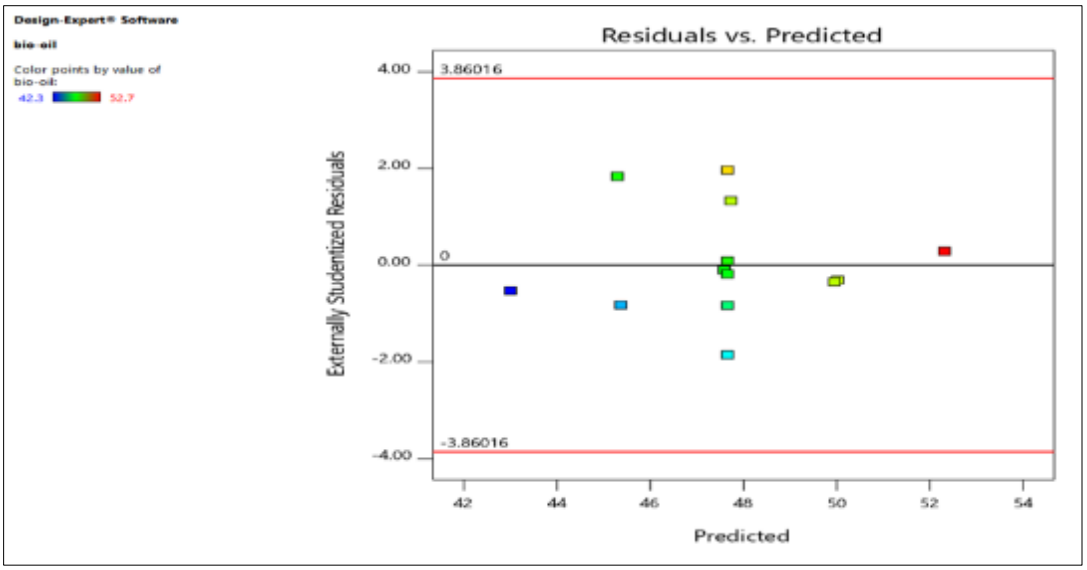

Figure 4 Plot of the Residuals against the Predicted value

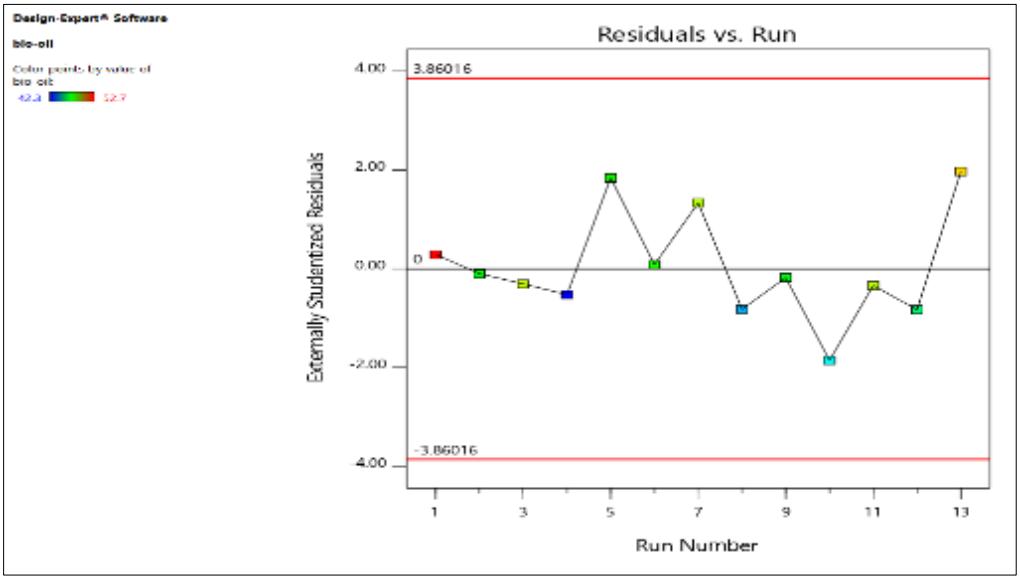

Figure 5 Plot of the Residual values against the Experimental Run

The model's projected values are the response values derived by including the independent values (Fig. 5).

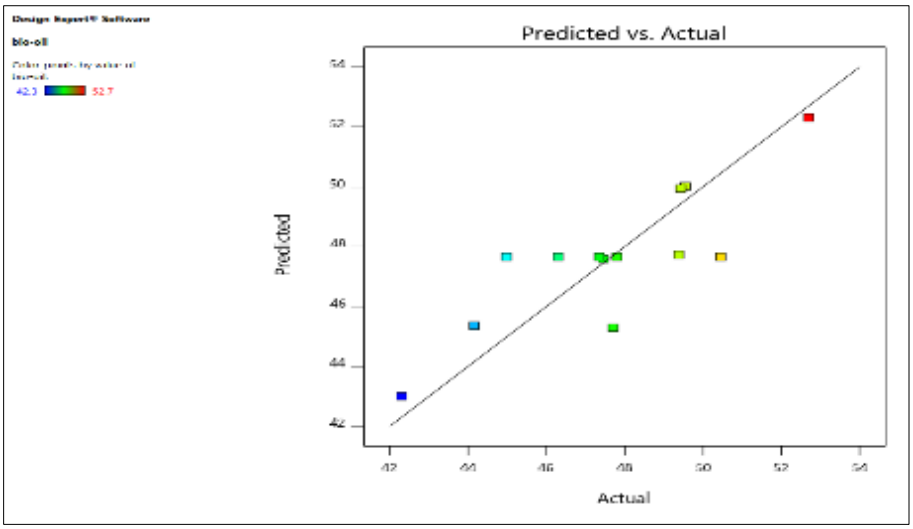

Figure 6 Plot of the Predicted values against the Actual values

The values are contrasted with experimental or actual values. As evidence of a strong correlation between the actual and expected values, it is seen that the relative distribution of the actual values is close to the expected values.

The normality probability plot of residuals could be used to verify the data's normality. It was discovered that the points fell along a straight line, demonstrating that the residuals are typically studentized. The assumption of constant variance is tested using the residual expected values. By dividing the residuals by the standard deviations, the studentized residuals are obtained (Ghafoori *et al.,* 2014). The randomly spaced points between the contour detection limits of -3 and +3 show that the generated models for bio-oil yield make very good predictions of the experimental results.

3.2.4. Main interactive effects of the variables on the pyrolysis process of the bio-oil yield produced

Figure 6 shows the 3D surface plot that illustrates the effects of each independent variable on the response variable (reaction temperature and reaction time on the bio-oil yield).

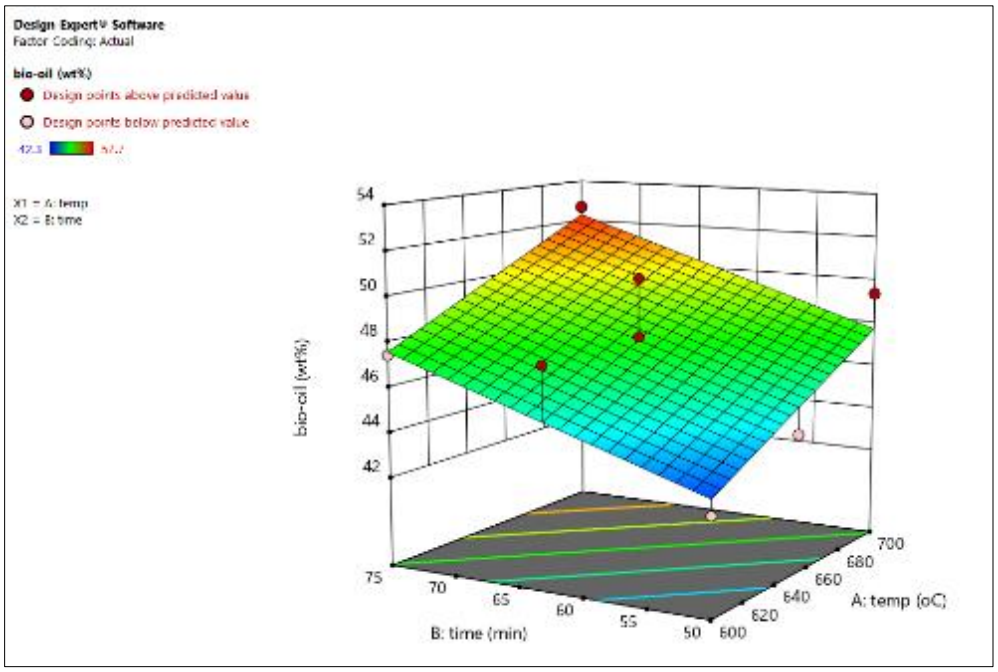

Figure 7 Interaction effect of reaction temperature and reaction time on the bio-oil yield of RPF

Figure 7 shows that temperature and reaction time interact together to affect the amount of bio-oil produced during pyrolysis when reaction time and temperature were varied. The temperature and reaction time axis were numbered in their coded values and in this plot, it shows that the reaction temperature and reaction time significantly affect the yield of the bio-oil. Also, in the graph, the results show that the yield of bio-oil increased with an increasing reaction temperature and reaction time at a temperature of 700 ^{o}C and 75 minutes which was required in achieving the maximum bio-oil output of 52wt%.

3.2.5. Process parameter optimization for the bio-oil

For maximum bio-oil yield, temperature and reaction time were optimized while remaining within the experimental parameters. From the optimisation data, the Design expert software's numerical optimisation tool produced one hundred (100) solutions, as indicated in Table 6

Table 6 Optimization data of the Bio-Oil

Name	Goal	Lower Limit	Upper Limit	Lower Weight	Upper Weight	Importance
A: temp	is in range	600	700	1	1	3
B: time	is in range	50	75	1	1	3
bio-oil	none	42.3	52.7	1	1	3

The software selected solution 1 with the most desirability (1.00) as the best result, which was validated experimentally, because the conditions of 671.53 ºC temperature, 62.41 min time to yield 48.66 %wt of bio-oil were more favorable as shown in Figure 5

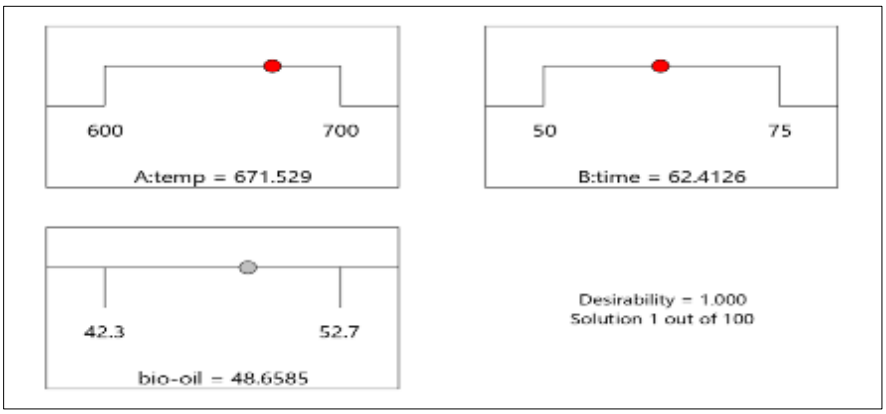

Figure 8 Ramps showing the optimal conditions needed for the highest bio-oil production from RPF

Pyrolysis experiments utilizing solution 1 were carried out under optimized conditions to verify the results. Table 6 provides an overview of the comparison of results (predicted and experimental outcomes).

Table 7 Experimental system selected yield verses experimentally validated yield at optimized process parameters

Temperature (^{o}C)		Time (min)		Yield of Bio-Oil	
Predicted	**Experimental**	**Predicted**	**Experimental**	**Predicted**	**Experimental**
671.53	670	62.41	62	48.66	50.12

The average bio-oil yield collected was 50.12 wt%. The experimentally validated values were found to be relatively distributed close to the experimental system's chosen values. The model appears to be adequate for predicting the results for maximal bio-oil yield because there is a little difference between the experimental results and predicted results from the model.

3.3. Characterization of Bio-Oil

3.3.1. Properties of Bio-Oil of Raffia Frond

Table 8 Properties of Bio-oil of OPF

Property	**Bio-oil**
	RF
Physiochemical property	
pH	3.3
Density (g/cm3)	1.005
Viscosity (cp)	6.2
Water content/moisture (wt %)	93.61
Volatile matter (wt %)	6.71
Ash content (wt.%)	0.17
Calorific value (mJ/kg)	2.07121
Ultimate analysis	
Carbon	15.16
Nitrogen	0.006
Sulphur	0.08
Hydrogen	26.16
Oxygen	58.51

From the pyrolysis of Raphia frond (RF) feedstock gave a dark brown bio-oil which was high in acidity, thereby indicating the presence of organic acids from lignin and hemicellulose breakdown (Abu and Titiloye, 2013; Fan *et al.,* 2014; Kan *et al.,* 2016). Also, in the result,—the bio-oil had a high-water content of 93.61 wt% due to dehydration/evaporation taking place during the pyrolysis (Zhang *et al.,* 2007). The result for density is 1.005 g/cm^3 and it is higher than that of gasoline and diesel. For viscosity, the result was 6.2 cp with ash content of 0.17 wt%, and this indicates they are potentially from metallic compounds or contaminants.

Ash contains metals like Ca, K, Si, and Fe (Asadullah *et al.,* 2008), which can lead to corrosion and equipment damage (Oasmaa and Peacock, 2001). The ultimate analysis revealed 15.16 wt% carbon, 26.16 wt% hydrogen, 0.006 wt% nitrogen, 0.08 wt% sulfur, and 58.51 wt% oxygen while the low sulfur and nitrogen levels suggest bio-oil is a relatively clean energy source. However, its low higher heating value of 2.071 MJ/kg compared to diesel (45 MJ/kg) and petrol (47 MJ/kg) is due to the high water and oxygen content, indicating a need for upgrading.

3.3.2. Fourier Transform Infrared Spectroscopy analysis

FTIR for Raffia Frond (RF)

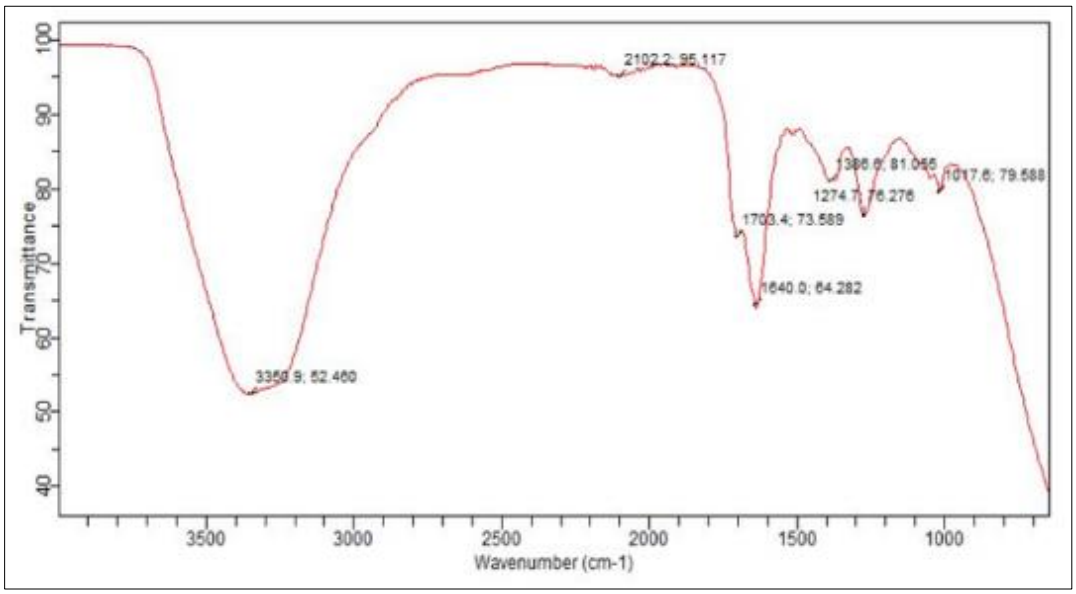

Figure 9 FTIR for Raffia frond at a temperature of 500 ^{0}C at 62.5 min

The FTIR analysis revealed several key functional groups in the bio-oil. A broad peak at 3,350 cm^{-1} indicates O–H stretching from hydrogen-bonded hydroxyl groups, suggesting the presence of phenols and alcohols (Fahma *et al.,* 2010). The peak at 1,703 cm^{-1} corresponds to C=O stretching, indicating carboxylic acids, ketones, and aldehydes from hemicellulose and lignin. A peak at 1,640 cm^{-1} shows C=C stretching, confirming the presence of alkenes from lignin. C–H deformation at 1,380 cm^{-1} suggests alkanes, while peaks at 1,274 cm^{-1} and 1,071 cm^{-1} indicate C–O stretching and C–OH groups, confirming alcohols, esters, ethers, and carboxylic acids.

3.3.3. GC-MS Analysis of Bio-Oil

GC-MS analysis of Bio-Oil from Raffia frond (RF)

Table 9 Chemical composition of Bio-Oil from Raffia frond at temperature of 700 ^{o}C

Header	PK	RT (min)	Area %	Library/ID	Ref	CAS	Qual
1	1	5.7888	3.6564	2-Fluorobenzoic acid. heptadecyl ester	226232	1000282-96-6	53
2	2	6.3616	9.7129	Phenol, 2,6-dimethoxy-	28298	000091-10-1	93
3	3	8.0896	48.4104	. beta. -D-Glucopyranose, 1,6-anhydro-	33655	000498-07-7	59
4	4	8.3083	9.245	n-Propyl heptyl ether	30655	071112-89-5	38
5	5	10.0618	7.0865	2-Pentanone, 1-(2,4,6-trihydroxyphenyl)	73956	1000116-22-3	64
6	6	13.91	0.8369	Bis(trifluoromethylthio)selenide	142297	153204-89-8	50
7	7	14.4817	13.2984	6H-1,3-Oxazin-6-one, 4-acetoxy-2-bromomethyl-	108843	1000158-71-5	43
8	8	14.5302	2.2076	n-Propyl 11-octadecenoate	182559	1000336-71-7	87
9	9	14.5759	1.6557	Octasiloxane, 1,1,3,3,5,5,7,7,9,9,11,11,13,13,15,15-hexadecamethyl-	272253	019095-24-0	45
10	10	14.6467	3.8904	Thymol, TBDMS derivative	124822	330455-64-6	70

The beta-D-glucopyranose, 1, 6-anhydro- was the most prevalent in the bio-oil (area percent, 48.41 %), followed by 6H-1,3-Oxazin-6-one, 4-acetoxy-2-bromomethyl- (area percent, 13.30 %), according to Table 9's raffia palm frond GC-MS results. Figure 10 displays the bio-oil from the raffia frond GC-MS Chromatograms.

The results demonstrated that the bio-oil chemical makeup is made up of several aromatic and oxygenated chemicals, including nitrogen, aldehydes, carboxylic acids, phenols, and ketones. The biomasses' biopolymer texture, which includes cellulose, hemicellulose, and lignin, was thought to be the cause of the occurrence of these aromatic and oxygenated chemicals. A prior study (Tsai, *et al.,* 2006) mentioned a few of these chemicals.

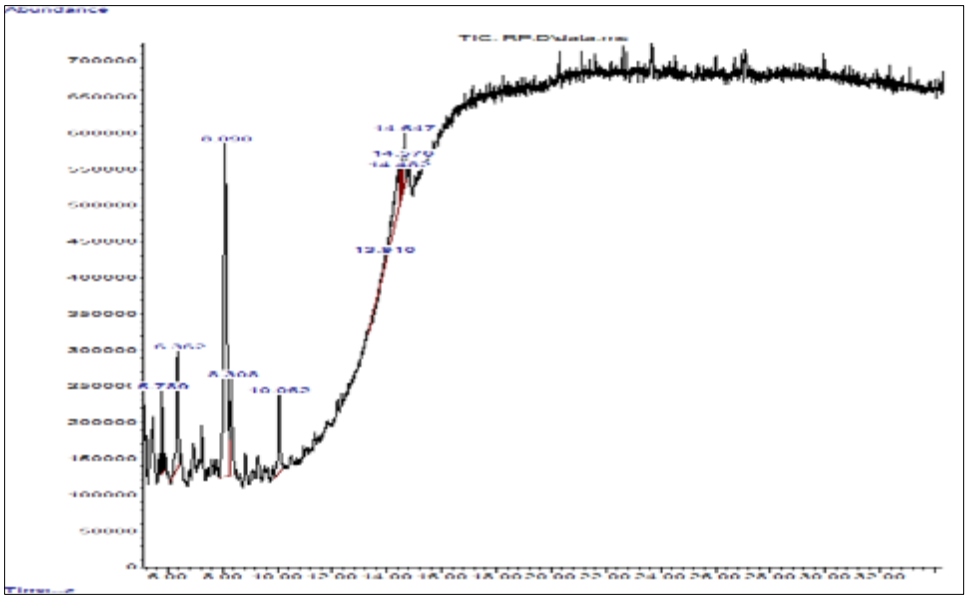

Figure 10 GC-MS chromatogram of Bio-Oil from Raffia frond at temperature of 700 °C

4. Conclusion

Pyrolysis of raffia frond was conducted in a fixed bed reactor and the products obtained were bio-oil, char and gas. According to this research, **t**he calorific value of the biomass was high (30.16 MJ/kg). The amount shows that the raw materials' energy content was appropriate for usage as a source of energy.

Bio-oil has a very high moisture content (93.61wt%). Water is important in several aspects; generally speaking, adding more water lowers viscosity, increases stability, and lowers heating value. Therefore, there is a need to reduce the water before it can be suitable as biofuel or chemical feedstock. The study indicates that bio-oil is acidic, having a pH value of 3.3. In the optimization studies for production of bio-oil from Raffia frond (RF), the ANOVA analysis indicated that the reaction temperature and time were significant, and the optimum point was at temperature of 700 °C, time of 75 mins and bio-oil yield of 52.31%.

The FTIR examination of all the functional groups found that oxygen predominates in the chemical component. Three different chemical components were found in ten raffia frond bio-oil, according to the GC-MS analysis. It was noted that the bio-oil's chemical composition corresponds to a mixture of several aromatic and oxygenated molecules, such as aldehydes, phenols, ketones, and carboxylic acids. The pyrolysis oil at this stage is best suitable as chemical feedstock.

Compliance with ethical standards

Disclosure of conflict of interest

No conflict of interest to be disclosed.

References

[1] Abu, M. S. and Titiloye, J.O. (2013). Catalytic Pyrolysis of Rice Husk for Bio-Oil Production. Journal of Analytical and Applied Pyrolysis, 103:362-368.

[2] Asadullah, M., Anisur, R. M., Mohsin, A. M., Abdul, M. M., Borhanus, S. M., Robiul, A. M. and Sahedur, R. M. (2008). Jute stick pyrolysis for bio-oil production in fluidized bed reactor. Bioresource Technology, 99 (1):44–50.

[3] Bhatia, S.K.; Bhatia, R.K.; Jeon, J.M.; Pugazhendhi, A.; Awasthi, M.K.; Kumar, D.; Kumar, G.; Yoon, J.J.; Yang, Y.H. (2021). An overview on advancements in biobased transesterification methods for biodiesel production: Oil resources, extraction, biocatalysts, and process intensification technologies. Fuel, 285, 119117. [CrossRef]

[4] Bridgwater, A. V. (2012). Review of fast pyrolysis of biomass and product upgrading. Biomass and Bioenergy, 38:68–94.

[5] Cardoso, C. A. L., Machado, M. E. and Caramão, E. B. (2016). Characterization of bio-oils obtained from pyrolysis of bocaiuva residues. Reneweable Energy, 91:21–31 doi: 10.1016/j.renene.2015.11.086.

[6] CBBR. (2010). "Biomass to gas, liquid and solid fuels: Green technology in the pipeline. UTP Green Technology Open Seminar, 14-15 June 2010, Kuala Lumpur.

[7] Fahma, F., Iwamoto, S., Hori, N., Iwata, T. and Takemura, A. (2010). Isolation, preparation, and characterization of nano fibers from oil palm empty fruit bunch (OPEFB). Journal of Cellulose, 17: 977–985.

[8] Fan, Y., Fowler, G. D., and Norris, C. (2017). Potential of a pyrolytic coconut shell as a sustainable biofiller for styrene–butadiene rubber. Industrial and Engineering Chemistry Research, 56 (16): 4779-4791.

[9] Ghafoori, S., Mehrvar, M, and Chan, P. K. (2014). A statistical experimental design approach for photochemical degradation of aqueous polyacrylic acid using photo-fenton-like process. Polymer Degradation and stability. 110, 492-497.

[10] International Energy Agency (IEA) (2023). n.d. http://iea.org/topics/bioenergy/

[11] Kan, T., Strezov, V. and Evans, T. J. (2016). Lignocellulosic biomass pyrolysis: A review of product properties and effects of pyrolysis parameters. Renewable and Sustainable Energy, 57:1126–40.

[12] Oasmaa, A. and Peacocke, C. (2001). A guide to physical property characterisation of biomass-derived fast pyrolysis liquids. VTT Publication, 2–65.

[13] Pinheiro Pires, A.P.; Arauzo, J.; Fonts, I.; Domine, M.E.; Fernández Arroyo, A.; Garcia-Perez, M.E.; Montoya, J.; Chejne, F.; Pfromm, P.; Garcia-Perez, M. (2019). Challenges and Opportunities for Bio-Oil Refining: A Review. Energy Fuels, 33, 4683–4720.

[14] Sarve, A., Varma, M. N. and Sonawane, S. S. (2015). Response surface optimization and artificial neural network modeling of biodiesel production from crude mahua (Mahua indica) oil under supercritical ethanol condition using CO2 as co-solvent. Royal Society of Chemists Advances. 5, 69702-69713.

[15] Sengar, H. S., Mohod, A. G. and Khandetod, Y. P. (2012). Performance Evaluation of Kiln for Cashew Nutshell Carbonization and Liquid. International Journal of Energy Engineering, 2 (3): 78-85.

[16] Tsai, W. T., Lee, M. K. and Chang, Y. M. (2006). Fast Pyrolysis of Rice Straw, Sugarcane Bagasse and Coconut Shell in an Induction-Heating Reactor. Journal of Analytical and Applied Pyrolysis, 76: 230-237.

[17] Wang, Y.; Li, B.; Gao, A.; Ding, K.; Xing, X.; Wei, J.; Huang, Y.; Chun-Ho Lam, J.; Subramanian, K.A.; Zhang, S. (2023). Volatile-Char Interactions during Biomass Pyrolysis: Effect of Biomass Acid-Washing Pretreatment. Fuel, 340, 127496.

[18] Zhang, Q., Chang, J., Wang, T. and Xu, Y. (2007) Review of Biomass Pyrolysis Oil Properties and Upgrading Research. Energy Conversion and Management, 48: 87-92.